Climate Dynamics (2019) 52:951–967
https://doi.org/10.1007/s00382-018-4174-7

On the effects of wildfires on precipitation in Southern Africa

Fernando De Sales[1] · Gregory S. Okin[2] · Yongkang Xue[2] · Kebonye Dintwe[3]

Received: 18 September 2017 / Accepted: 12 March 2018 / Published online: 16 March 2018

Abstract
This study investigates the impact of wildfire on the climate of Southern Africa. Moderate resolution imaging spectroradiometer derived burned area fraction data was implemented in a set of simulations to assess primarily the role of wildfire-induced surface changes on monthly precipitation. Two post-fire scenarios are examined namely non-recovering and recovering vegetation scenarios. In the former, burned vegetation fraction remains burned until the end of the simulations, whereas in the latter it is allowed to regrow following a recovery period. Control simulations revealed that the model can dependably capture the monthly precipitation and surface temperature averages in Southern Africa thus providing a reasonable basis against which to assess the impacts of wildfire. In general, both wildfire scenarios have a negative impact on springtime precipitation. September and October were the only months with statistically significant precipitation changes. During these months, precipitation in the region decreases by approximately 13 and 9% in the non-recovering vegetation scenario, and by about 10 and 6% in the recovering vegetation wildfire scenario, respectively. The primary cause of precipitation deficit is the decrease in evapotranspiration resulting from a reduction in surface net radiation. Areas impacted by the precipitation reduction includes the Luanda, Kinshasa, and Brazzaville metropolitan areas, The Angolan Highlands, which are the source of the Okavango Rive, and the Okavango Delta region. This study suggests that a probable intensification in wildfire frequency and extent resulting from projected population increase and global warming in Southern Africa could potentially exacerbate the impacts of wildfires in the region's seasonal precipitation.

1 Introduction

Wildfires play an important role in determining global and regional climate, as they are capable of changing the land surface's physical, chemical, and biological characteristics. They occur in every continent except in Antarctica (Roy et al. 2008; Bowman et al. 2009) and are integral part of many ecosystems (Bond et al. 2005). However, they are particularly prevalent in Africa, where 9% of the land is estimated to burn annually, and 22% of the continent burns every 8 years during the fire season (Barbosa et al. 1999). It is estimated that Africa's wildfires are responsible for approximately 70% of the global burned area (Andela and van der Werf 2014).

The most obvious component of wildfire is its effect on vegetation. Post-fire landscapes are characterized by deposits of charred material and changes in distribution of living and dead biomass, both of which can result in prolonged changes to the surface albedo and Bowen ratio (Samain et al. 2008; Bowman et al. 2009; French et al. 2016; Dintwe et al. 2017). Therefore, extensive burned areas have the potential to cause significant changes to heat and moisture exchanges between the biosphere and the lower troposphere, and consequently result in alterations to patterns of wind and precipitation. Nevertheless, studies on the impacts of wildfire-induced change on wind circulation and precipitation are scarce and tend to focus on regions where the annual precipitation is primarily driven by monsoons (Gorgen et al. 2006; Lynch et al. 2007; De Sales et al. 2016).

Wildfires are also sources of aerosols and black carbon to the atmosphere, which in turn, can affect air quality and cloud formation (Haywood et al. 2008; van der Werf et al.

✉ Fernando De Sales
fdesales@mail.sdsu.edu

[1] Department of Geography, San Diego State University, San Diego, CA, USA

[2] Department of Geography, University of California Los

convective activity, especially in the afternoon, leading to an average daily precipitation decrease in South America. Tummon et al. (2010) investigated the direct and indirect radiative effects of biomass burning and dust aerosol over southern Africa during the austral winter season. Wildfire-induced aerosol emissions were found to cause changes in regional surface fluxes and atmospheric dynamics. Surface radiative forcing decreased by up to 60 W m^{-2} over the major burn regions, resulting in decreased surface turbulent fluxes and temperatures.

There have been limited efforts to quantify the effects of burned areas on Africa's climate. The modeling study by De Sales et al. (2016) examined the role of wildfires on precipitation in the Sahel region. The study found that burned areas were responsible for a decrease in rainfall due to the cooling and drying of atmosphere, which consequently led to a weakening in convective activity and precipitation. Most of the wildfire impacts on rainfall were observed during the pre-monsoon season. Modeling studies on the impact of burned areas in Southern Africa have been particularly lacking.

Saha et al. (2016) compiled 15 years of satellite data to quantify the effects of wildfires on precipitation in Africa. The study concluded that more extensive and later dry season fires tend to lead to rainfall deficits of up to approximately 10% in the wet season over the continent. This effect was particularly strong in Southern Africa, a fact that the authors attributed to the fires there occurring mainly later in the dry season than in other regions of the continent. Additionally, the study suggested the existence of a coupling between rainfall, fuel load, and wildfire in the drylands of southern Africa, whereby wildfire-suppressed precipitation would result in a reduction in fuel load and thus wildfire in the subsequent season. The reduced burned areas would then enhance rainfall completing the feedback loop.

The present study aims to assess the effects of wildfire on the surface climate precipitation in Southern Africa through a series of regional climate model simulations. To accomplish this task, the WRF-ARW regional climate model (Skamarock et al. 2008) was implemented with the second version of the Simplified Simple Biosphere (SSiB-2) vegetation biophysical processes model (Xue et al. 1991; Zhan et al. 2003). Daily burned area fraction, calculated from MODIS approximate-date-of-burning product (MCD45), was incorporated in the simulations to guide the evolution and extent of the fire season in the region during the simulations.

Two different post-fire vegetation scenarios are explored in this study. The first consists of a series of simulations wherein the vegetation is not allowed to regrow after a fire so time. These two post-fire scenarios are referred to as non-recovering (NOREC) and recovering (REC) vegetation scenarios, respectively.

2 The model, burned area data and experimental design

2.1 The model

The experiments for this study were performed using the weather research and forecasting (WRF) regional modeling system (Skamarock et al. 2008). More specifically, the Advanced Research version of WRF (ARW) was selected for the study due to its broader array of physics schemes available, which should allow for higher-complexity investigations in the future including the role of wildfires on atmospheric radiation exchanges. The ARW is an advanced fully compressible model built upon a system with terrain-following hydrostatic pressure vertical and staggered Arakawa C-grid-type horizontal coordinates. The model offers many physics scheme options and is maintained and supported by the Mesoscale and Microscale Meteorology Division of NCAR.

The model domain was set up on a 30-km horizontal resolution grid with 38 vertical levels centered at 20°E and 20°S, covering Southern Africa and the adjoining oceans (Fig. 1). Preliminary short-term simulations were conducted to test the physics options available in the model over Southern Africa. Based on these tests, the following physics schemes were selected: Ferrier microphysics scheme (Ferrier 1994), the Fu–Liou–Gu shortwave and longwave radiation schemes (Gu et al. 2011), Yonsei University PBL scheme (Hong et al. 2006), and Grell–Devenyi convective scheme (Grell and Devenyi 2002).

For land surface processes, the SSiB-2 model was implemented into the ARW. The SSiB-2 is a state-of-the-art vegetation biophysical model that estimates photosynthesis-controlled land surface processes, while preserving energy, water and momentum conservation at the atmosphere-land surface interface (Zhan et al. 2003). Hereafter, the atmosphere-land surface coupled model will be referred as ARW/SSiB2. Distribution of land cover types in the model domain is shown in Fig. 1. Climatological monthly MODIS-derived leaf area index and vegetation cover fraction were used as surface boundary conditions in the simulations.

2.2 Burned area data

The MODIS approximate date-of-burning product (MCD45) available at the University of Maryland, College Park, web-

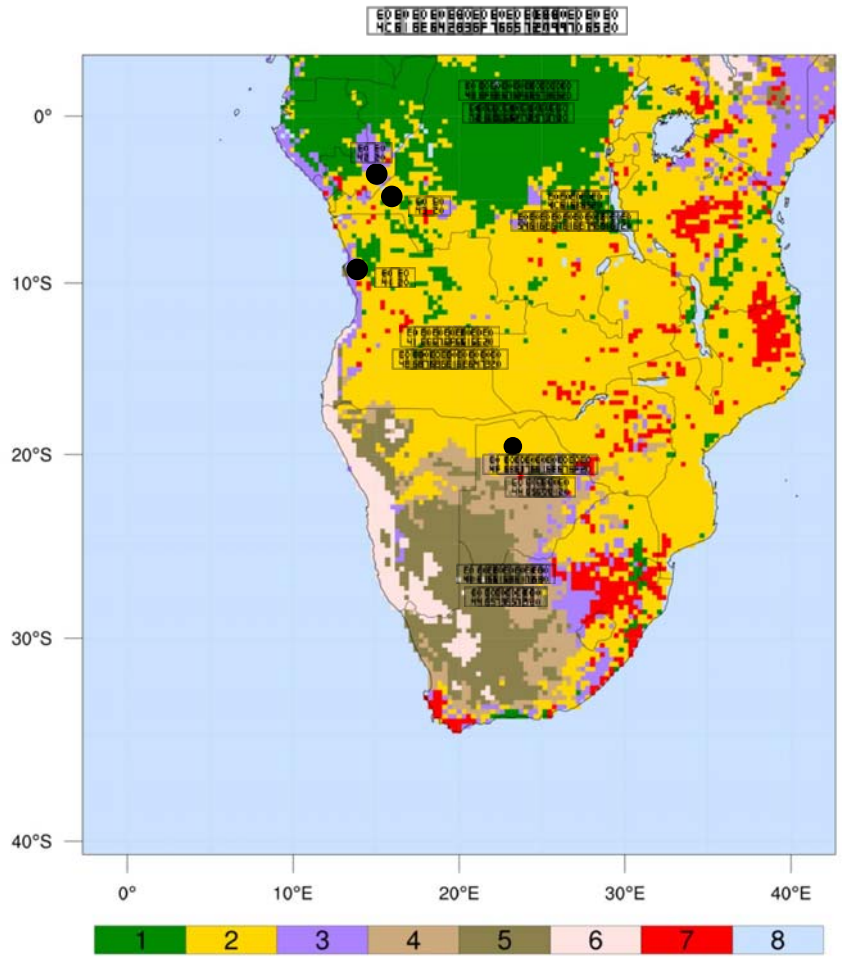

Fig. 1 The domain used for the WRF-ARW/SSiB2 simulations and its land cover type distribution. Land cover types are (1) rainforest, (2) savanna, (3) grasslands, (4) shrubs on grass, (5) shrubs on bare soil, (6) bare soil, (7) cropland, and (8) water. The location of the metropolitan areas of (A) Luanda, (B) Kinshasa, and (C) Brazzaville, and of the Angolan highlands, Congolese rainforest, Lake Tanganyika, Okavango Delta, and Kalahari Desert are also indicated

burning, which are obtained by locating the occurrence of rapid changes in daily surface reflectance time series data as described by Roy et al. (2002, 2008).

The methodology to obtain burned area fraction from MCD45 data is described in detail in the work by De Sales et al. (2016). In summary, high-resolution monthly unburned-burned binary masks derived from MCD45 files, between 2002 and 2013, were aggregated into 30-s resolution fractional burned area maps using a grid-cell averaging method. The 12-year-mean monthly fractional burned area maps were then calculated and implemented in the ARW/SSiB2 model. Finally, daily burned-area fraction is calculated for each grid cell during model run-time using a simple linear interpolation scheme.

This approach is chosen to minimize the effects of missing information resultant from those periods when the Burned areas are evident throughout the domain from May to October (Fig. 2). During these months, hereafter referred as wildfire season, most of the domain experiences some wildfire except the very southern portion of the Kalahari Desert and the Congo rainforest region (between 5°S and 15°S and 10°E and 30°E). The most impacted regions are located in Central Africa between 20°S and 5°S extending from the Atlantic Coast to Lake Tanganyika. Another region with significant amounts of burned areas are observed along the Eastern Coast from East Lake Malawi southward into South Africa. Through the wildfire season, burned areas seem to start and intensify in the northwest section of the domain and slowly progress towards the southeast. Little wildfire activity is observed during the wet season from November to April.

By combining the information on Figs. 1 and 2, the

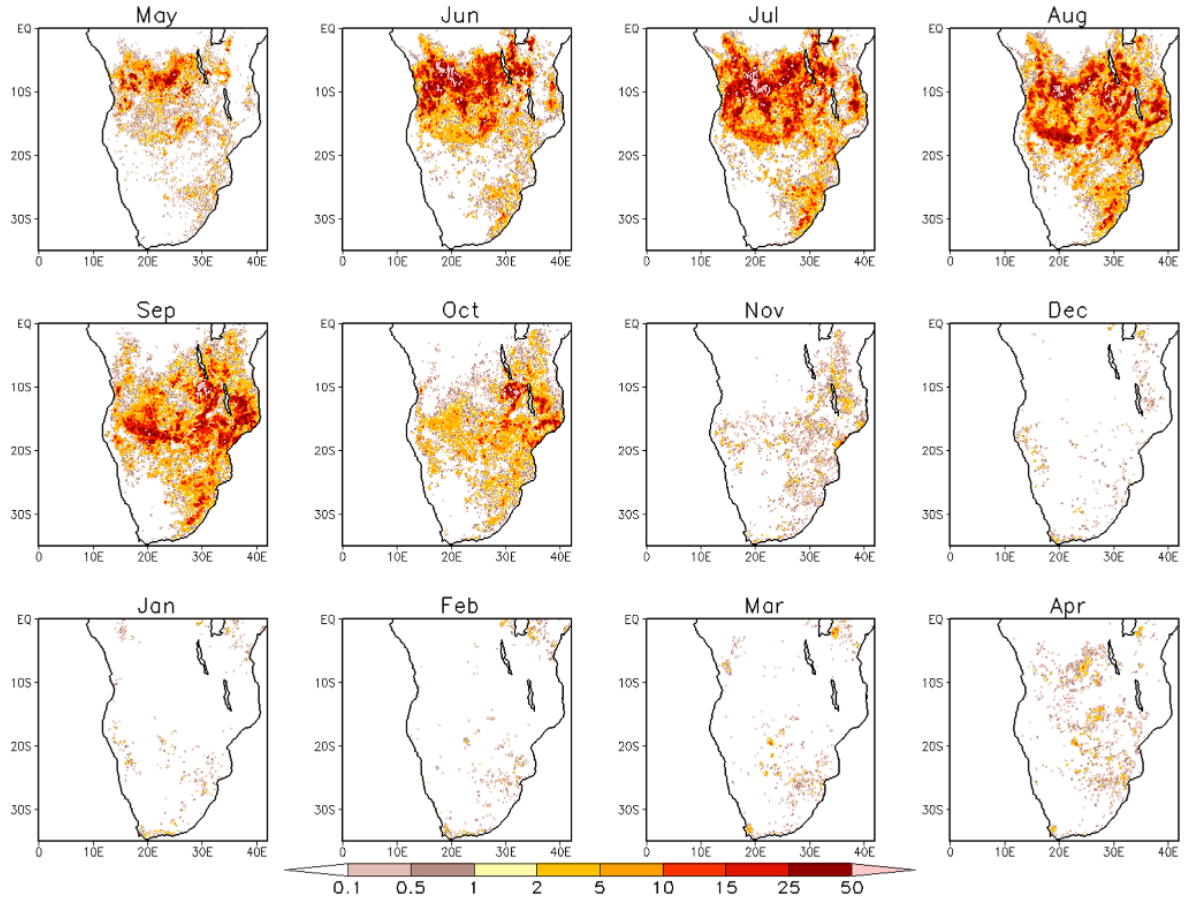

Fig. 2 Average monthly burned area fraction calculated based on MODIS approximate date of burning product aggregated from the native resolution to the model grid

Table 1 Cover fraction, annual burned area fraction, survival rate, and relative albedo change in burned areas during wildfire season for the major land cover types in the study area

Land cover type	Area (%)	Annual burned area fraction (%)	Survival rate (%)	Relative albedo change in burned areas (%)
Savannas	54.5	18.9	15.0	4.6
Shrublands	17.1	1.2	0.0	7.9
Forests	12.7	4.3	75.0	1.0
Croplands	6.3	16.8	0.0	3.0
Grasslands	5.5	4.2	0.0	0.0
Bare ground	3.8	–	–	0.0

approximately 54.5% of the land, followed by shrublands (17.1%), forests (12.7%), croplands (6.3), and grassland (5.5%). Based on the SSiB2 vegetation map, the approximate amount of burned areas for each of these land cover

the particular horizontal resolution used in this study, the vegetation types most impacted by wildfires are savannas and croplands. However, from the perspective of areal extent, by far savannas dominate the burned areas as crop-

2.3 Experimental design

Three sets of experiments are conducted to investigate the impact of burned area on the climate of meridional Africa (Table 2). In the first set, wildfire effects are not included and land surface properties were maintained undisturbed throughout the model integrations. This is referred to the unburned or control experiment.

The impact of wildfires on vegetation and soil are included in the second and third sets of experiments. In these, leaf area index (LAI) and vegetation cover fraction were altered every 24 h based on the daily burned area fraction described above and on the prescribed survival rates of the vegetation type. For instance, LAI was altered following Eq. 1, where LAI_u, FBA, and SR represent the unburned LAI, fractional burned area, the survival rate, respectively.

$$\text{[illegible]} \quad (1)$$

A similar formula was used to reduce vegetation cover. The resulting vegetation reduction, thus, depends not only on the fraction of burned area but also upon vegetation survivorship (Table 1). The vegetation survival rates used in this study are similar to estimates described in the work by De Sales et al. (2016).

The main difference between second and third experiments is the treatment of post-fire vegetation recovery. In the former, once burned vegetation remains degraded until the end of simulations, while in the latter vegetation is allowed to grow back to its undisturbed state. These results are referred to as non-recovering (NOREC) and recovering (REC) vegetation experiments, respectively (Table 2).

The non-recovering vegetation experiment follows the methodology described in the work by De Sales et al. (2016), which examines the effect of wildfires in Sub-Saharan Africa without post-fire vegetation regrowth. In addition to altering the vegetation, soil reflectance was lowered based on the same amount of burned area fraction and survival rate to simulate the effect of ash and charcoal depositions associated with wildfires (Govaerts et al. 2002; Samain et al. 2008). Ground darkening was maintained for a period of 45 days [a compromise value between those reported by Samain et al. (2008) and by Dintwe et al. (2017)] after which the soil albedo was returned to its unburned values to mimic the action of char removal by wind and precipitation. During the soot residence period, shortwave and near-infrared ground albedos were arbitrarily set to 0.1 over the burned fraction of the grid cell to simulate ground darkening. This value is consistent with recent post-fire albedo found in Africa by Govaerts et al. (2002).

Lastly, the recovering-vegetation (REC) experiment was designed to investigate the role of vegetation regrowth on the wildfire impacts in the region (Simon and Pennington 2012; du Toit et al. 2015; Dintwe et al. 2017). In these simulations, the burned vegetation was restored to its unburned value following a vegetation-recovering period of 140 days. Ash and char deposition and removal followed the same methodology described for the non-recovering experiments. However, unlike the NOREC experiments, the land albedo was allowed to return to its undisturbed value as the contribution of exposed bare ground was cancelled by post-fire vegetation regrowth. As the date and extent of burning vary throughout the region, LAI and VCF in the NOREC and REC experiments are not identical during the wildfire season. The 140-day vegetation recovery time was obtained from the work by Dintwe et al. (2017), in which pre and post-fire albedo and enhanced vegetation index are used to determine the vegetation recovery in Southern Africa.

A five-member ensemble of simulations was performed for each of three experiments to reduce uncertainties associated with the initial conditions. No form of nudging was utilized for the simulations, which were carried out continuously without any restarts. The ensemble members were initialized at 00z 01, 02, 03, 04 and 05 March 2012 and ended at 00z 01 May 2014. NCEP-DOE Reanalysis 2 (Kanamitsu et al. 2002) data was used as initial and boundary conditions in all simulations, as well as sea surface temperature information. The first two months of simulation are assigned as model spin-up and thus are not included in the analysis. All reported results are based on the 5-member ensemble averages of the experiments.

Table 2 Summary of experiment descriptions

Experiment	Description	Char and ash	Vegetation	Start date of ensemble members
Control	Benchmark experiment	None	Undisturbed	00z 01 Mar 2012 00z 02 Mar 2012 00z 03 Mar 2012 00z 04 Mar 2012 00z 05 Mar 2012
NOREC	Non-recovering vegetation wildfire experiment	Stays on the burned soil for 45 days following fire, then is completely removed	Remains degraded after fire until the end of simulation	
REC	Recovering-vegetation wildfire experiment	Same as NOREC	Remains degraded for 140 days after a fire, after which	

3 Results

3.1 Control simulations

Since this study is the first publication that describes results obtained with the ARW/SSiB2 modeling system, we first evaluate the control experiment to establish a benchmark for assessing the impact of wildfire-induced land degradation on climate in Southern Africa. 2012–2013 monthly average precipitation and surface air temperature results are compared to the University of Delaware observational analysis (Legates and Willmott 1990a, b) to evaluate the model's spatial performance in the region. We select these two variables because they are good indicators for overall performance in simulating wind circulation and moisture transport, as well as land–atmosphere interactions such as canopy radiation transfer and land surface energy balance.

Early in the dry season (May to September), precipitation concentrates over the rainforest region in the northern portion of the domain between the Equator and 10°S. During those months, weak precipitation is observed in the extreme south and southeast regions, and nearly no precipitation is registered in the central portion of the study area (Fig. 3). As the transition from dry to wet season commences in October, points with rainfall above 100 mm month^{-1} start to expand southward and then southeastward into central region. By December, a large northwest-southwest band of monthly total with at least 200 mm month^{-1} is observed across central Africa and most of the domain experiences precipitation. The lowest precipitation totals during this month are found in the southwest regions of the continent, including the Kalahari Desert.

As the wet season progresses, the area of maximum precipitation shifts further to the east and by January it is located along the central Indian Ocean coast between 10°S and 20°S. February signals the start of the wet season withdrawal. Precipitation decreases significantly throughout the

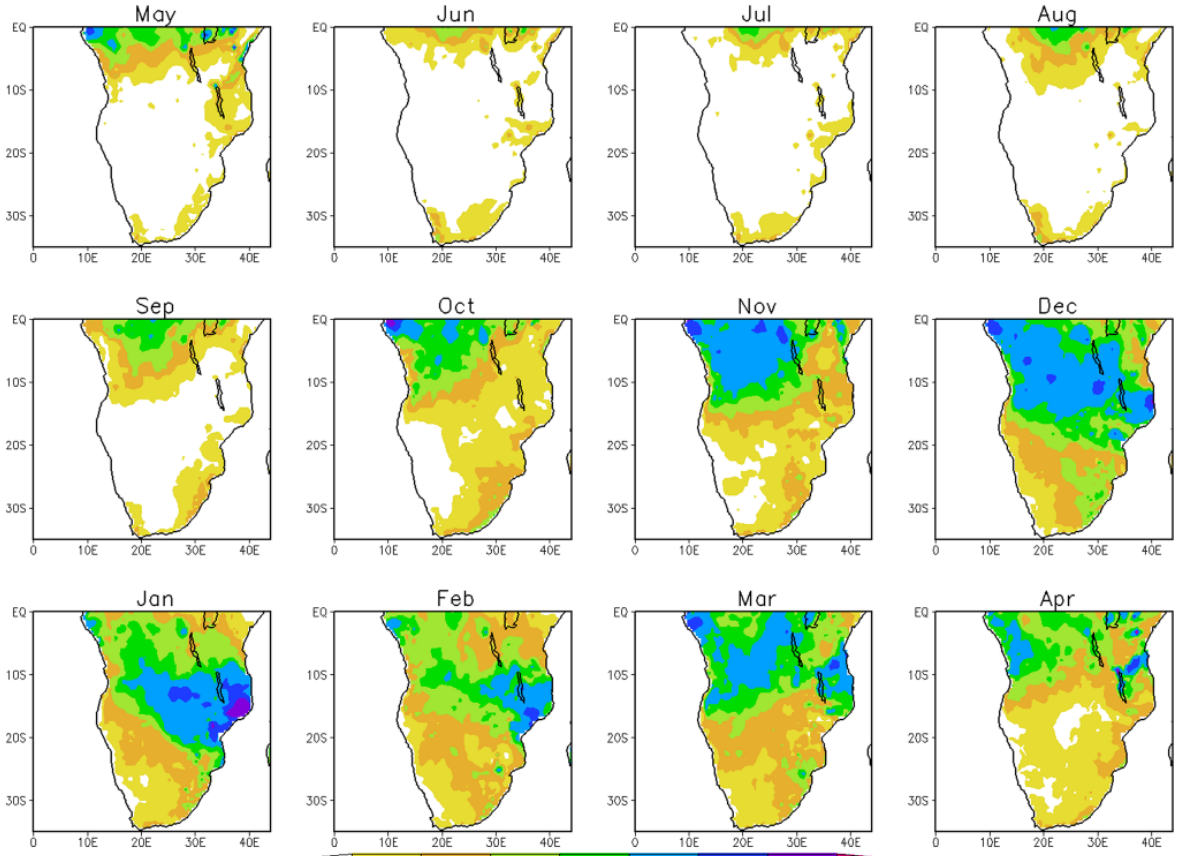

continents, and it starts to retreat to the north and northwest (Fig. 3). Precipitation distribution in April is similar to that in October with most of rainfall concentrated in the northwest region of the domain, except however for a few areas of intense-precipitation recorded in April in the area between the African great lakes and the Indian Ocean (Fig. 3).

In general, the ARW/SSiB2 model is able to simulate the main features of monthly precipitation distribution in Southern Africa, including the main seasonal variability modes described above. The simulations capture the initially southern and later easterly progression of the precipitation across the land during the wet season, despite overestimating the precipitation total in some locations. One area where the model consistently overestimates precipitation is over the highlands of eastern South Africa. It simulates well the spatial distribution of precipitation during the wet months of December and January, as well as the rainfall northwest retreat from February to April (Fig. 4).

Domain-average monthly and annual bias, root-mean-square error, and spatial correlation coefficient between modeled and observed precipitation provide to assess model's performance (Table 3). On the annual average, the model overestimates the precipitation by about 9.7 mm month^{-1}. The annual average root-mean-square error and spatial correlation coefficient for the domain are respectively 30.6 mm month^{-1} and 0.80. The largest errors occurred in the wettest months from December to February, while the lowest spatial correlations are in May and August when rainfall is limited to the northern domain boundary.

Observations of surface air temperature reveal a warming progression similar to precipitation moving southward then eastward and finally southwestward from northwest corner of the domain (Fig. 5). The warmest areas are located along latitude 20°S in spring, and in the Kalahari Desert and along the Indian Ocean coast during the summer months. The extreme south experiences the greatest seasonal temperature changes. Temperatures there vary from below 10 °C in the winter to above 25 °C in the summer.

The model simulates surface air temperature reasonably well, with all main features being represented (Fig. 6).

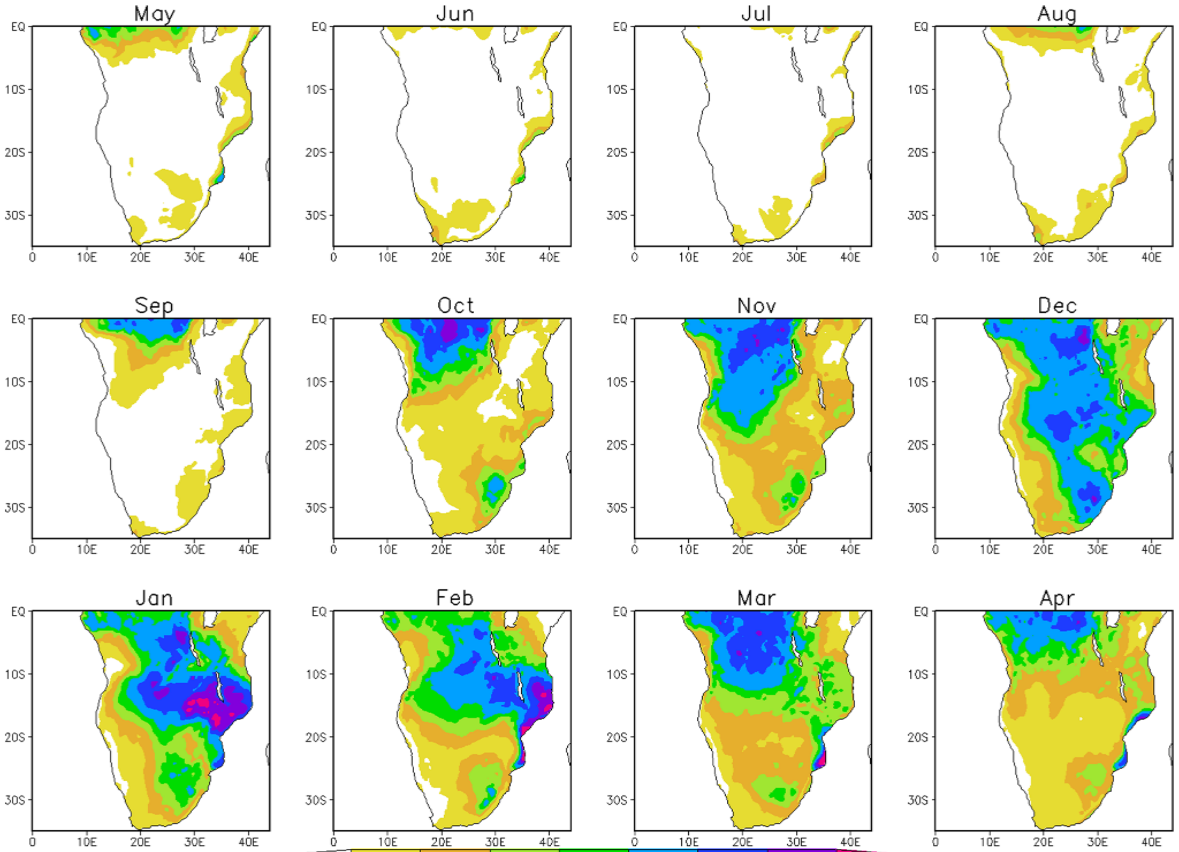

Table 3 Model performance for monthly and annual mean precipitation and surface air temperature compared to UDEL observations between May 2012 and Apr 2014 averaged over land points between 0°–35°S and 10°E–40°E Bias, Rmse and Scor represent respectively the bias, root-mean-squared error (mm month^{-1} and °C), and spatial correlation coefficient

Variable	Metric	May	Jun	Jul	Aug	Sep	Oct	Nov	Dec	Jan	Feb	Mar	Apr	Ann
Precipitation	Bias	− 9.2	0.5	− 0.4	− 4.3	− 7.6	13.5	19.8	17.2	36.1	37.6	8.4	4.8	9.7
	Rmse	32.9	14.3	10.4	18.71	19.7	43.2	59.0	87.4	87.9	82.4	76.0	56.8	30.6
	Scor	0.3	0.6	0.6	0.4	0.9	0.9	0.8	0.5	0.8	0.8	0.6	0.6	0.8
Surface air temperature	Bias	− 0.8	− 1.5	− 1.3	− 1.0	− 0.4	0.1	0.5	1.0	0.6	0.3	0.2	0.0	0.0
	Rmse	2.2	2.8	2.6	2.5	2.0	1.8	2.1	2.2	1.9	1.8	1.8	1.8	1.7
	Scor	0.9	0.9	0.9	0.9	0.9	0.9	0.8	0.7	0.7	0.7	0.7	0.8	0.8

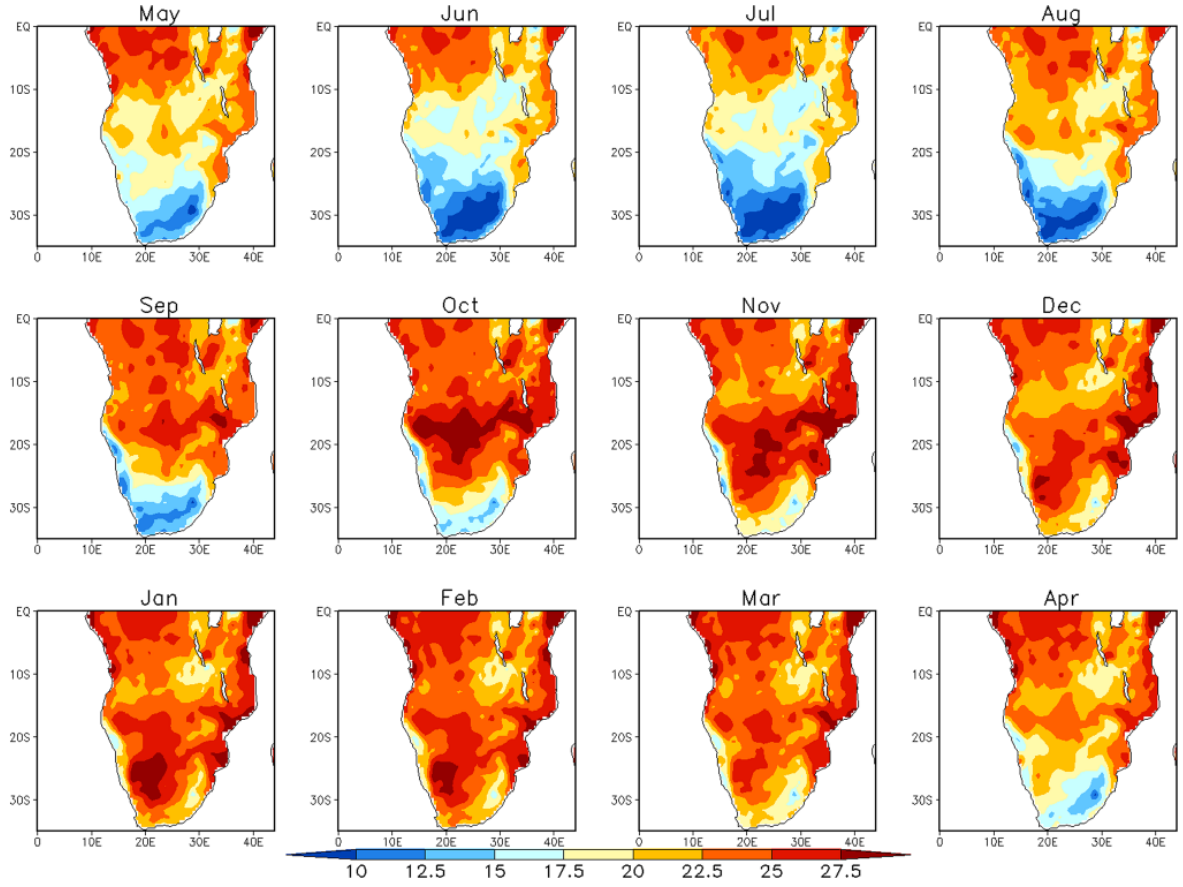

Fig. 5 May 2012–Apr 2014 observed monthly average surface air temperature (°C)

Modeled winter temperatures in the south are colder than the observed. On the other hand, modeled summer temperatures along the Indian Coast are warmer than observations. Nevertheless, the warming progression from the spatial correlation in the domain based on the observations are equal to 0.0, 1.7, and 0.8 °C respectively. The largest spatial errors occur in the winter months.

The work by Diallo et al. (2015) indicates that obser-

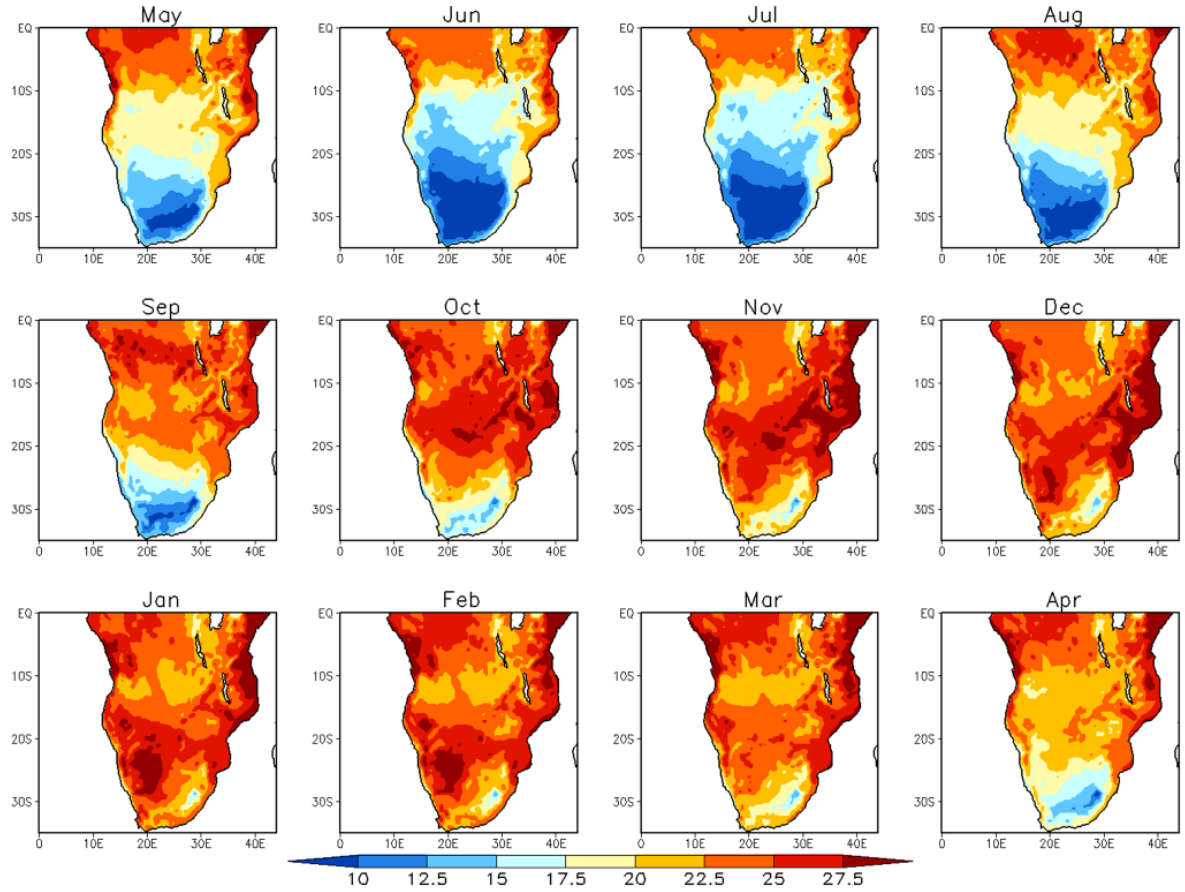

Fig. 6 Same as Fig. 5, except showing control–case simulation results

annual cycle to other observational datasets, namely: the Global Telecommunication System (Chen et al. 2008), the Tropical Rainfall Measuring Mission (Huffman et al. 2007), and the University of East Anglia Climatic Research Unit (Harris et al. 2013) analyses (Fig. 7). In general, the simulations capture the transitions from dry to wet season and from cold to warm months observed in Southern Africa. The wettest months in both observation and simulation are December and January, while the driest are June and July. Despite the larger uncertainty in precipitation observations, the model consistently overestimates rainfall totals between during the wet season (Fig. 7a). Uncertainties are much smaller among observed surface temperature data sets, and for most part, modeled temperature results fall within the observational range. A slight cold bias persists during the winter, however (Fig. 7b).

Overall, these results reveal that the ARW/SSiB2 vegetation degradation in the region's energy balance and precipitation.

3.2 Non-recovering burned area impacts

Before looking at the consequences of wildfires on the climate, we look at the impact of wildfire on vegetation. As discussed in the Sect. 2.2, most of wildfires in the domain take place during the dry season between May and October. Therefore, most of impacts of fire on soil and vegetation take place during that period.

Under undisturbed conditions, changes to surface albedo are often associated with changes in topsoil moisture content and vegetation phenology. As a result, maximum average albedo values are often reached by the end of dry season, followed by a slow decline during the wet season. On the other hand, under wildfire-disturbed conditions, two other distinct

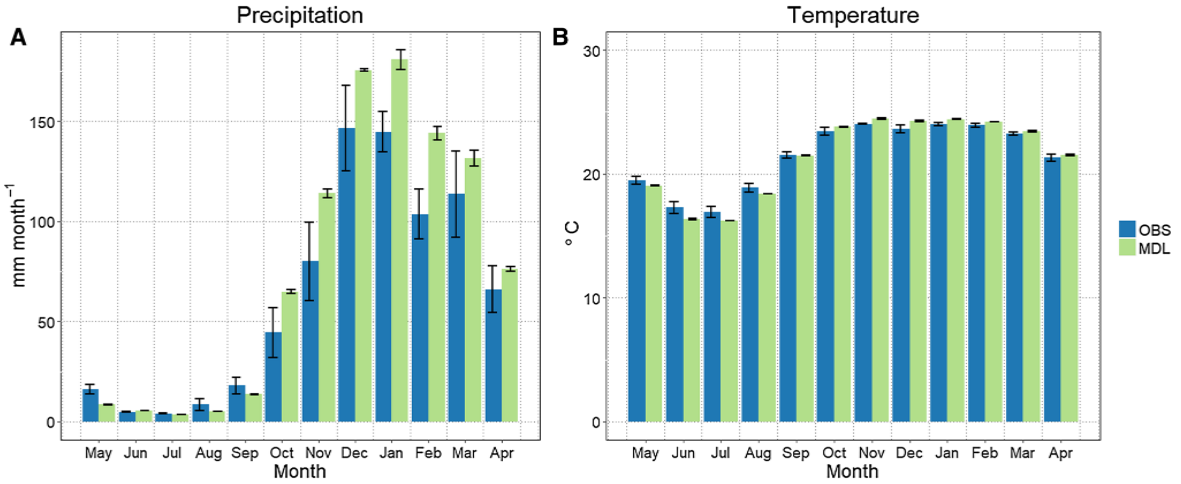

Fig. 7 Annual cycles of observed (OBS) and modeled (MDL) monthly mean precipitation and surface air temperature over the study area (0–35°S and 10°E–40°E). Error bars indicate one standard deviation among observational datasets and model ensemble members (mm month^{-1} and °C)

Therefore, during the dry season, as vegetation cover is reduced with increasing burned areas, larger and larger portions of bare ground become directly exposed to solar incoming radiation. Despite the brief ground darkening from soot deposition following wildfires, the model simulations indicate that the resulting effect is to increase the average surface albedo in the areas where bare ground albedo is higher than the overlying vegetation reflectance.

In the model, shrublands and savanna experience the largest albedo change, with a 7.9 and 4.6% relative increase due to wildfire-induced land degradation compared to unburned experiments (Table 1). Over croplands and forests, albedo increases by 3.0 and 1.0%, respectively. No albedo change was simulated over grasslands as this land cover is mainly located in sections of the domain where little or no burned areas are observed in the MODIS data. Overall, relative albedo changes are smaller than described by De Sales et al. (2016) for the Sahelian region of Africa. Annual fractional burned areas in the Sahel are indeed larger than in Southern Africa (Fig. 2, De Sales et al. 2016).

Annual changes in the surface radiation balance are consistent with the increase in albedo, as indicated by a decrease in surface net radiation over the burned areas (Fig. 8a). Larger decreases are observed where burning and land degradation was greater, especially in the areas south of the Congo rainforest regions (between 5°S and 15°S and 15°E and 25°E) where net radiation dropped by more than 8 W m^{-2} in some spots. Large changes in surface net radiation are observed also to the east and southwest of Lake Tanganyika and Central Angola. No statistically significant

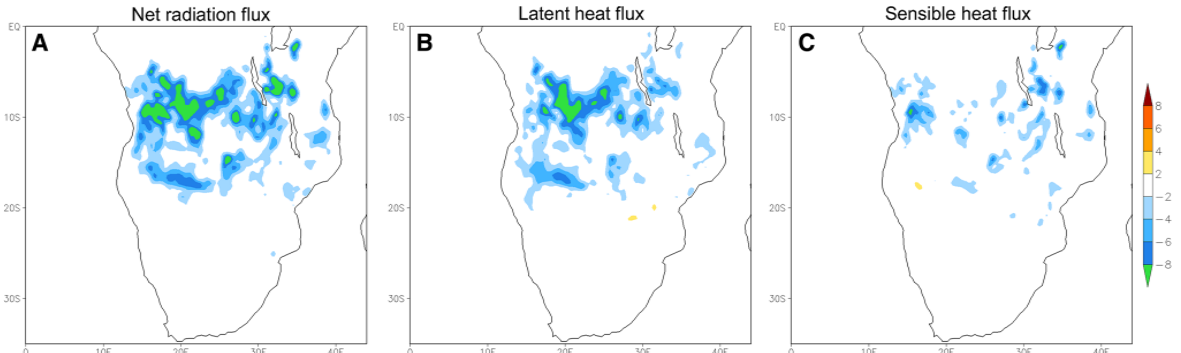

changes (> 90%-level of confidence) are observed outside burned areas.

At annual time scales, changes in net radiation should equate to changes in sensible and latent heat fluxes. The partitioning between these two types of heat flux depends on soil and vegetation properties as well as on air temperature and humidity gradient between the surface and the surrounding air. In general, the changes associated with the burned areas favored changes in latent over sensible heat flux on the region (Fig. 8b, c). Most of the decrease in surface available energy is associated with the reduction in surface evapotranspiration along with very small changes in convective heat transfer. Overall, the wildfire-induced albedo increase and evapotranspiration decrease resulted in minor surface temperature warming over the burned areas (not shown).

Differences in the net radiation components, namely downward and upward shortwave (SWD, SWU), and downward and upward longwave (LWD, LWU) radiation, between the control and burned experiments provide further information on the impacts of NOREC wildfires on the surface energy partitioning (Fig. 9a). Of the four components, LWU experiences the greatest changes with an increase of 37 W m^{-2} per year on average. Most of this change occurs between July and November, when it increases by about 26 W m^{-2}. SWU and SWD follow with annual increase of 20 W m^{-2}. Between September and January, the amount of shortwave radiation reflected by the surface increase by approximately 5% on average over the burned areas. LWD is the only component that experiences a decrease, however small, between August and October.

LWU increases every month, with the largest changes observed in late winter and early spring, and reflect the decrease in surface evapotranspiration and could be enhanced by ground darkening following wildfire. On the other hand, most of the impacts on SWU take place in the spring and early summer, and are primarily due to the rise in bare ground exposure after fires. These can be considered direct effects of wildfires on climate.

In contrast, the LWD decrease and SWD increase observed are probably secondary effects resulting from the atmospheric drying over the burned areas (Fig. 8b). By reducing the flux of latent heat from the surface, wildfires lead to drier atmospheric conditions and less cloud cover over burned areas, which consequently result in less atmospheric thermal emittance and more incoming solar radiation at the surface (Fig. 9a).

The consequences of these changes in radiation balance and energy fluxes at the surface can also be evaluated through the analysis of the atmospheric water balance (Table 4; Fig. 10a). At monthly time scales, average precipitation can be estimated from two moisture sources: surface evapotranspiration and atmospheric moisture flux convergence (MFC). Precipitation, evapotranspiration, and MFC for the control experiment are shown in Fig. 10a for reference. Under undisturbed conditions, dry-season evapotranspiration and MFC partially cancel each other out to keep precipitation low. From October to March, this pattern changes as MFC becomes positive and starts to contribute to precipitation, along with increasing evapotranspiration. April's evapotranspiration is the primary source of precipitation that month as MFC is at a minimum (Fig. 10).

NOREC wildfires cause a consistent reduction in monthly evapotranspiration, which is particularly strong in late winter and spring seasons (Table 4). Monthly evapotranspiration

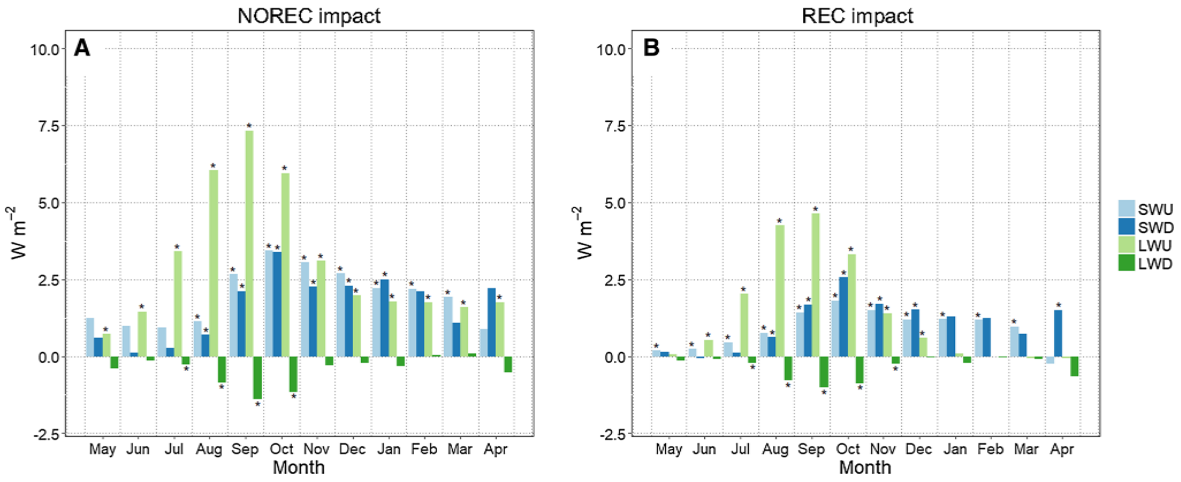

Table 4 Impact of NOREC and REC wildfires on monthly and annual average precipitation (PRC), evapotranspiration (EVP), and moisture flux convergence (MFC) (mm month^{-1})

Scenario	Variable	May	Jun	Jul	Aug	Sep	Oct	Nov	Dec	Jan	Feb	Mar	Apr
NOREC	PRC	−0.2	0.0	0.0	−0.1	**−**	**−**	−0.8	−1.2	−0.6	−0.1	1.1	−0.5
	EVP	−1.0	−1.0	**−**	**−**	**−**	**−**	**−**	**−**	−0.9	−0.9	−1.0	−1.7
	MFC	0.8	1.0	**0.8**	**0.8**	**0.5**	**−**	0.3	0.1	0.2	0.9	2.1	1.1
REC	PRC	0.0	0.0	0.0	0.0	**−**	**−**	−1.9	−0.5	−2.0	−0.9	−0.8	−1.2
	EVP	−0.3	−0.5	**−**	**−**	**−**	**−**	−0.9	−0.4	−0.4	−0.3	−0.1	−0.9
	MFC	0.3	0.5	**0.6**	**0.5**	**0.3**	**−**	−1.0	−0.2	−1.6	−0.6	−0.6	−0.3

Values in bold are statistically significant at a 90% confidence level

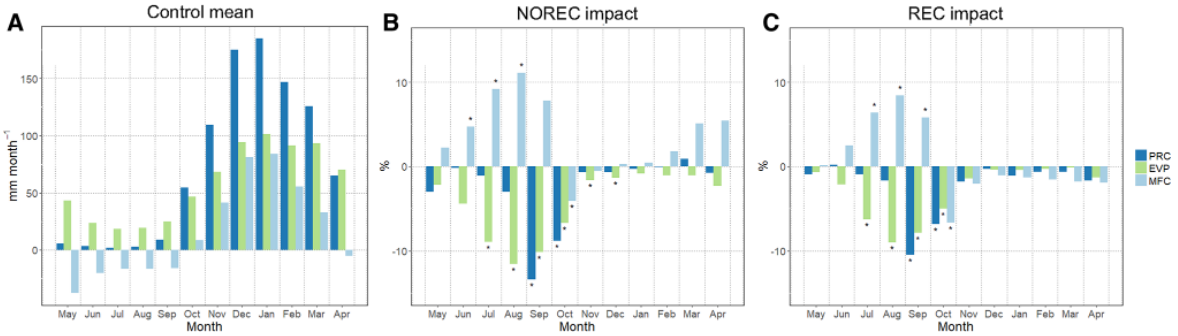

Fig. 10 Control monthly mean of precipitation (PRC), evapotranspiration (EVP), and vertically-integrated moisture flux convergence (MFC) over the domain. Show the relative difference between NOREC and REC experiment and control, respectively (mm month^{-1} and %). Asterisks indicate that the difference is statistically significant at a 90% confidence level (see Table 4)

drops on average by 9.0, 12, and 10% in July, August, and September respectively compared to control simulations. During these months, atmospheric moisture flux divergence predominates over the region, and the effect of burned areas was to weaken the existing divergent conditions, probably because of warmer surface conditions in NOREC (Fig. 9). Precipitation also decreases almost every month following the drop in evapotranspiration. However, only September and October show statically significant results. October is also the only month when both evapotranspiration and MFC contribute to the monthly precipitation decrease.

Figure 10b shows the impact of NOREC fires on the water balance components in relation to the control scenario results. The purpose is to emphasize the impact of burned areas on the annual cycle. Relative to the undisturbed scenario, most of rainfall reduction occurs in August, September, and October when the monthly rainfall totals approximately 3.0, 13.4, and 9.0% less than that observed in the control experiments. These months represent the tail end of the dry season, a period when water availability is usually low. A decrease in precipitation during that time of year has a potentially stronger impact for the region than during the with a reduction in evapotranspiration, despite the increase in MFC in some months. For instance, between August and November, the domain-average changes in precipitation, evapotranspiration, and MFC are roughly -6.9, -9.0, $+1.9$ mm month^{-1}, respectively. These results differ from similar experiments carried out for the Sahel region, where most of the precipitation change was associated with a decrease in atmospheric moisture flux convergence (De Sales et al. 2016).

Figure 11a shows the precipitation difference between NOREC and control experiments for the months whose difference is statistically significant. Most of the area affected by the rainfall deficit is concentrated over northern the northwestern areas, including most of Lake Tanganyika, and the large metropolitan centers of Luanda, Kinshasa, and Brazzaville (Fig. 1). The areas most affected are those located to the west of 30°E and north of 10°S, where rainfall decreases of over 20 mm month^{-1} are observed in some points. When averaged over the impacted area, the NOREC scenario generated 11% less precipitation than the control experiment. A few areas along the southeastern sector of the domain, however, experience an increase in

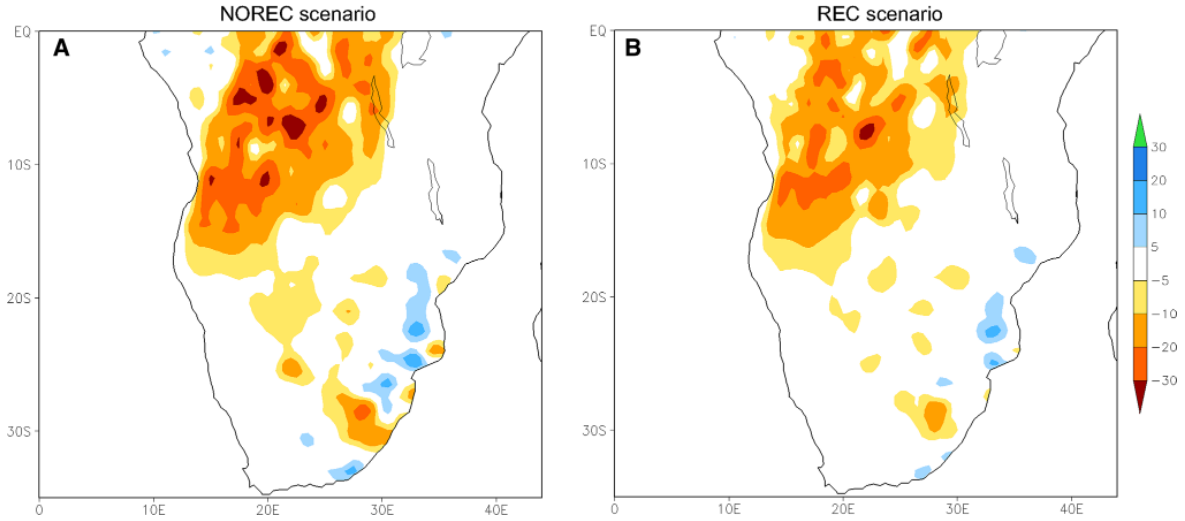

Fig. 11 September–October average precipitation difference caused by wildfire-induced land degradation on NOREC and REC scenarios. Only differences statistically significant at a 90% confidence level are shown (mm month^{-1})

3.3 The role of vegetation recovery

The wildfire impacts discussed so far arise primarily from changes in albedo associated with changes in vegetation cover and in top soil moisture content. In those experiments, however, once a patch of vegetation is burned, it remains so until the end of the simulation.

The recovering-vegetation (REC) experiment is intended to reveal information on the role of post-fire vegetation recovery on the wildfire impacts (Table 2). In these simulations, vegetation is allowed to grow to its original state 140 days following a fire (Dintwe et al. 2017). As vegetation recovers, the contribution of exposed bare ground in the burned areas decreases and the surface albedo begins to reflect the albedo of vegetation. It should be mentioned that the dominant grid-cell vegetation type is not changed due the fire in these experiments, so that the original land cover type map still applies (Fig. 1).

REC wildfires leads to changes in net radiation, latent and sensible heat fluxes that are spatially similar to those for NOREC fires (not shown). Moreover, changes in SWU, SWD, and LWD radiation components also follow similar timing. However, vegetation recovery lowers the overall radiative impact by nearly 35% compared to NOREC (Fig. 9b). One particular difference in the REC scenario is the lack of LWU impact during the wet season, indicating that vegetation regrowth is crucial for maintaining summertime surface temperatures.

for the rainfall deficit is a decrease in monthly evapotranspiration. Similarly, only September and October precipitation changes, −10% and −6% respectively, are statistically significant (Table 4). NOREC and REC scenarios produce similar September–October average precipitation impact patterns, with the latter showing a weaker signal (Fig. 11b). The areas most affected are mainly the same as in the non-recovery vegetation scenario. When spatially averaged over the impacted area, vegetation recovery generated 25% more precipitation than NOREC during those two months.

4 Discussion

The two sets of experiments, NOREC and REC, discussed in Sect. 3 can be classified as two extreme wildfire scenarios. In the first, burned vegetation remains completely removed after fire; and in the second, it regenerates completely after a recovery period. From a climatic perspective, the occurrence of either scenario is primarily controlled by precipitation interannual variability, as rainfall is a main regulator to vegetation regrowth. Other factors such as the effects of wildfire on soil nutrient concentration and changes in nutrient uptake are relevant, but are beyond the scope of this study (Van Der Vijver et al. 1999; Wilson et al. 2015).

We hypothesize that in drier years, conditions could favor the non-recovering vegetation situation, with a stronger decrease on precipitation. Whereas, wetter years should sup-

results shown here are a sound estimate of the impact of wildfire-induced degradation in Southern Africa and that on average years, a combination of NOREC and REC outcome should occur.

NOREC and REC atmospheric water balances suggests that the primary cause of precipitation reduction is a drop in evapotranspiration associated with the decrease in surface net radiation. Such a reduction is particularly large in September and October, which marks the end of the fire season when the impacts of water availability decline are probably of greater consequence. On average, NOREC and REC burned areas reduce the Sep-Oct mean precipitation by approximately 10.0% and 8.0%, respectively, in the study area.

Surface latent heat flux is crucial for the formation of clouds and precipitation in tropical and subtropical latitudes, as it helps enhance the planetary boundary layer air buoyancy, thus promoting the development of a potentially convective environment even in the absence of strong baroclinic conditions. The effects of reduced evapotranspiration on convective precipitation can thus be measured by its impact on the atmospheric convective stability (CS), calculated as the equivalent potential temperature gradient between lower (850 hPa) and middle (500 hPa) levels of the troposphere. Convectively unstable conditions (CS < 0 °C) exists when the mid-levels of the troposphere are dry and high dew-point temperatures are present near the surface. When the atmosphere is convectively unstable, wet convection and precipitation are likely.

Vegetation degradation caused by wildfires increases the atmospheric stability in September and October in the region (Fig. 12a). The distribution of convective stability in the control experiment shows that the atmosphere over the burned areas is predominantly unstable, with a CS median value around −4 °C, in September and October. Most of the convectively unstable points are location towards the central and northwestern portions the domain (not shown). NOREC fires tend to shift the distribution toward positive values or more stable atmospheric conditions. NOREC median CS is approximately −0.4 °C. Wildfires followed by vegetation recovering also stabilizes the atmosphere, however, less effectively than the non-recovering scenario.

Prevailing low-level winds over the burned areas in September and October are southeasterly and easterly (Fig. 12b). These winds advect the more stable air masses over burned areas toward the west and northwest regions of Southern Africa, where most of the precipitation-deficit areas are found (Fig. 12). The advective process results in reduced precipitation in areas where little to no wildfire are registered including the Congolese rainforest and the Angolan Coast.

In addition to affecting the regional water cycle, wildfires also influence the amount of carbon fixed by vegetation in southern Africa (Fig. 13). Both wildfire scenarios result in a decrease in gross primary production (GPP) on average over study area. While NOREC wildfires cause GPP to decrease every month, the recovering-vegetation scenario limits the impact to the dry season months. The annual average change in GPP for the NOREC and REC scenarios is approximately −6.4 and −3.2%, respectively.

It should be noted that the results presented here might be strongly dependent on the methodology used to describe the

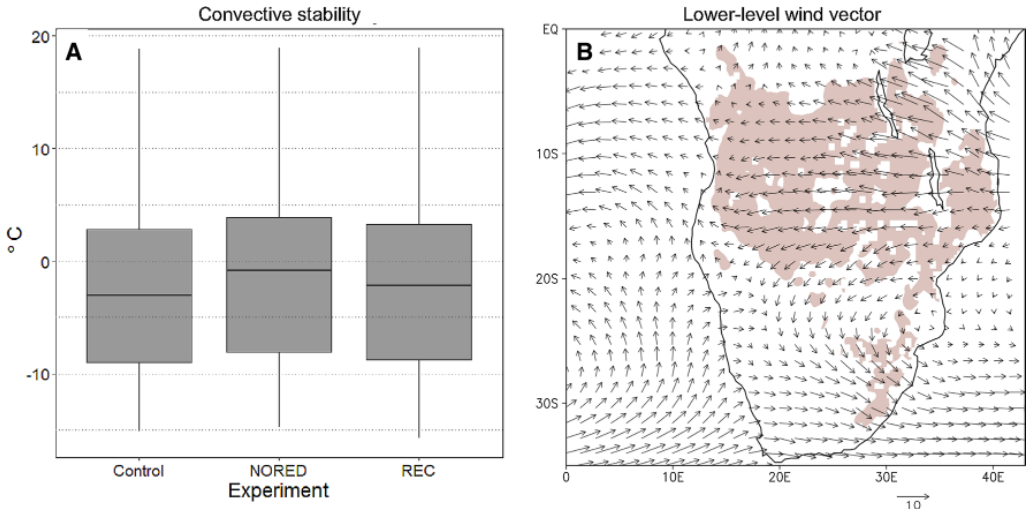

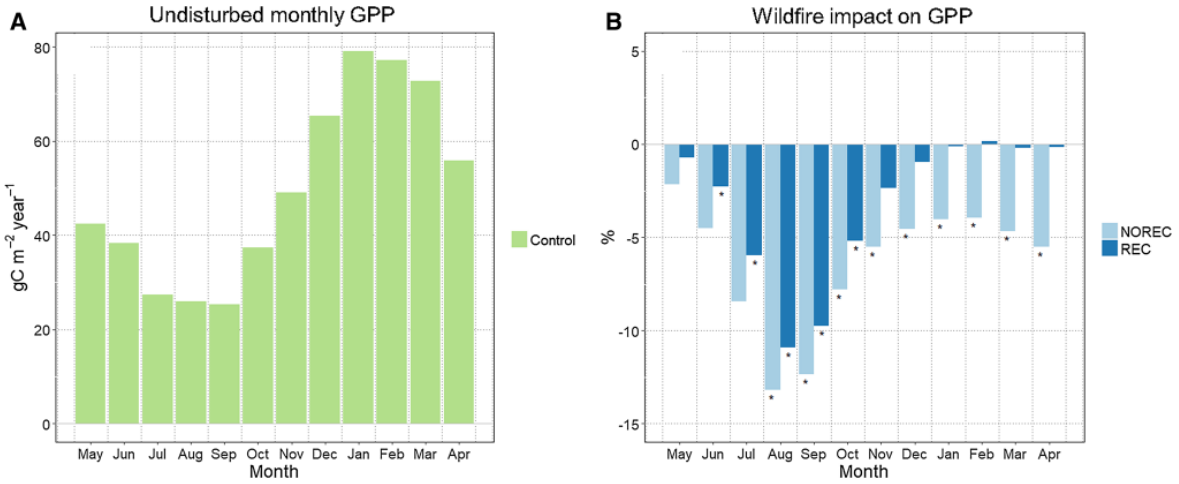

Fig. 13 Control–case monthly gross primary productivity, and monthly relative difference between control and NOREC and REC wildfire experiments. Asterisks indicate that differences that are statistically significant at a 90% confidence level (gC m^{-2} year^{-1} and %)

effect of fire on the vegetation and soil, including the timing of soil and vegetation post-fire recoveries (Table 2). The study by Dintwe et al. (2017) indicates that post-fire vegetation and soil albedo recovery timing in southern Africa may be different from those used in this study. In that study, wildfires results in a prolonged decrease in albedo, which is believed to be associated with the lingering of charcoal and ash on the ground after the wildfire. They conclude that surface runoff and wind in Southern Africa may not be as effective charcoal and ash dispersers as commonly assumed, causing the ground to remain darker for a long period following a fire.

Wildfires are part of the natural seasonal cycle of growth, decay, and combustion of vegetation in Southern Africa, and they can be ignited by lightning strikes as well as by anthropogenic activities. With the population and temperature in many southern Africa's countries predicted to increase in the next decades (United Nations 2015; IPCC 2014), one should expect an increase in wildfires. Our results suggest that these projections could potentially lead to further decrease in rainfall and gross primary productivity in Southern Africa.

5 Concluding remarks

This study highlighted some of the impacts of wildfires as well as the roles of post-fire vegetation recovery on the surface climate and precipitation of Southern Africa. Two post-fire scenarios were investigated: in the first once model can dependably simulate monthly precipitation and surface temperature averages in southern Africa thus providing a reasonable basis against which to assess the impacts of wildfire.

The NOREC and REC scenarios ultimately resulted in either a permanent or a temporary increase of average surface albedo due to the removal of vegetation by fire, which consequently caused a drop in surface net radiation available over the burn areas. The reduced amount of available energy at surface induced a reduction in evapotranspiration, which subsequently resulted in a decrease in atmospheric convective instability and a drop in precipitation in the burned areas as well as downwind locations for in scenarios. Changes to the surface radiation components showed clear monthly responses to ash deposition, increased bare ground exposure, and atmosphere drying caused by wildfires.

Although nearly every month observed some precipitation change, only September and October yielded statistically significant changes. Average September and October monthly precipitation dropped by approximately 13 and 9% in the non-recovering vegetation experiments, and by roughly 10 and 6% on average throughout the region. Areas affected by precipitation deficit include northern the northwestern areas of Southern Africa, to where burned-area induced more stable air mass was advected. Some large metropolitan areas impacted include Luanda, Kinshasa, and Brazzaville. The Angolan Highlands, which are the source of the Okavango River, and the Okavango Delta are also impacted (Fig. 1). When averaged over the impacted area,

September and October represent the trail end of the dry season in Southern Africa, a period when water availability is frequently limited. A decrease in precipitation during that time of year has a potentially stronger impact for the region than during the rainy season. In addition to impacting the water cycle negatively, wildfires also influenced the gross primary production in the region. The annual average change in GPP for the NOREC and REC scenarios was approximately −6.4 and −3.2%, respectively. Most of this changes occurred during the dry season.

Future projections indicate a steady increase in temperature and population in Southern Africa, which could potentially enhance the wildfire activity. The quantification of the wildfire impacts on the surface climate and precipitation, and their implications for terrestrial carbon fluxes are of scientific importance to our understanding of the present and future climate of Southern Africa.

Acknowledgements This study was funded by NASA Grant NNX-11AQ16G. The authors would like to thank NCAR Computational and Information System Laboratory (CISL) for providing invaluable computer time for the model simulations. All the model runs described in this study were carried out at the NCAR CISL Yellowstone high-performance cluster.

References

Andela N, van der Werf GR (2014) Recent trends in African fires driven by cropland expansion and El Nino to La Nina transition. Nat Clim Change 4(9):791–795

Barbosa PM, Stroppiana D, Gregoire JM, Pereira JMC (1999) An assessment of vegetation fire in Africa (1981–1991): Burned areas, burned biomass, and atmospheric emissions. Glob Biogeochem Cycles 13(4):933–950

Bond WJ, Woodward FI, Midgley GF (2005) The global distribution of ecosystems in a world without fire. New Phytol 165(2):525–537

Bowman D, Balch J, Artaxo P, Bond W, Carlson J, Cochrane M, D'Antonio C, DeFries R, Doyle J, Harrison S, Johnston F, Keeley J, Krawchuk M, Kull C, Marston J, Moritz M, Prentice I, Roos C, Scott A, Swetnam T, van der Werf G, Pyne S (2009) Fire in the earth system. Science 324:481–484

Chen M, Shi W, Xie P, Silva VBS, Kousky VE, Wayne Higgins R, Janowiak JE (2008) Assessing objective techniques for gauge-based analyses of global daily precipitation. J Geophys Res 113:D04110. https://doi.org/10.1029/2007JD009132

De Sales F, Xue YK, Okin GS (2016) Impact of burned areas on the northern African seasonal climate from the perspective of regional modeling. Clim Dyn 47(11):3393–3413

Diallo I, Giorgi F, Sukumaran S, Stordal F, Giuliani G (2015) Evaluation of RegCM4 Driven by CAM4 over Southern Africa: mean climatology, interannual variability and daily extremes of wet season temperature and precipitation. Theo Appl Climatol 121:749–766. https://doi.org/10.1007/s00704-014-1260-6

Dintwe K, Okin GS, Xue YK (2017) Fire-induced albedo change and du Toit JCO, van den Berg L, O'Connor TG (2015) Fire effects on vegetation in a grassy dwarf shrubland at a site in the eastern Karoo, South Africa. Afr J Range Forage Sci 32(1):13–20

Ferrier B (1994) A double-moment multiple-phase 4-class bulk ice scheme. 1. Description. J Atmos Sci 51(2):249–280

French NHF, Whitley MA, Jenkins LK (2016) Fire disturbance effects on land surface albedo in Alaskan tundra. J Geophys Res Biogeosci 121(3):841–854

Gorgen K, Lynch AH, Marshall AG, Beringer J (2006) Impact of abrupt land cover changes by savanna fire on northern Australian climate. J Geophys Res 111. https://doi.org/10.1029/2005jd006860

Govaerts YM, Pereira JM, Pinty B, Mota B (2002) Impact of fires on surface albedo dynamics over the African continent. J Geophys Res Atmos 107. https://doi.org/10.1029/2002JD002388

Grell GA, Devenyi D (2002) A generalized approach to parameterizing convection combining ensemble and data assimilation techniques. Geophys Res Lett 29(14):38-1–38-4. https://doi.org/10.1029/2002gl015311

Gu Y, Liou KN, Ou SC, Fovell R (2011) Cirrus cloud simulations using WRF with improved radiation parameterization and increased vertical resolution. J Geophys Res 116. https://doi.org/10.1029/2010jd014574

Harris I, Jones PD, Osborn TJ, Lister DH (2013) Updated high-resolution grids of monthly climatic observations—the CRU TS3.10 Dataset. Int J Climatol. https://doi.org/10.1002/joc.3711

Haywood JM, Pelon J, Formenti P, Bharmal N, Brooks M, Capes G, Chazette P et al (2008) Overview of the dust and biomass-burning experiment and African monsoon multidisciplinary analysis special observing period-0. J Geophys Res 113. https://doi.org/10.1029/2008JD010077

Hong SY, Noh Y, Dudhia J (2006) A new vertical diffusion package with an explicit treatment of entrainment processes. Mon Weather Rev 134(9):2318–2341

Huffman GJ, Adler RF, Bolvin DT, Gu G, Nelkin EJ, Bowman KP, Hong Y, Stocker EF, Wolff DB (2007) The TRMM multi-satellite precipitation analysis: quasi-global, multi-year, combined-sensor precipitation estimates at fine scale. J Hydrometeor 8(1):38–55

IPCC (2014) Climate change 2014: synthesis report. In: Core Writing Team, Pachauri RK, Meyer LA (eds) Contribution of working groups I, II and III to the fifth assessment report of the intergovernmental panel on climate change. IPCC, Geneva, p 151

Kanamitsu M, Ebisuzaki W, Woollen J, Yang S, Hnilo J, Fiorino M, Potter G (2002) NCEP-DOE AMIP-II reanalysis (R-2). Bull Am Meteorol Soc 83(11):1631–1643

Legates DR, Willmott CJ (1990a) Mean seasonal and spatial variability in gauge-corrected, global precipitation. Int J Climatol 10(2):111–127

Legates DR, Willmott CJ (1990b) Mean seasonal and spatial variability in global surface air temperature. Theor Appl Climatol 41(1–2):11–21

Lynch AH, Abramson D, Gorgen K, Beringer J, Uotila P (2007) Influence of savanna fire on Australian monsoon season precipitation and circulation as simulated using a distributed computing environment. Geophys Res Lett 34(20). https://doi.org/10.1029/2007gl030879

Roy D, Lewis P, Justice C (2002) Burned area mapping using multi-temporal moderate spatial resolution data—a bi-directional reflectance model-based expectation approach. Remote Sens Environ 83(1–2):263–286

Roy DP, Boschetti L, Justice CO, Ju J (2008) The collection 5 MODIS burned area product - Global evaluation by comparison with the MODIS active fire product. Remote Sens Environ

Samain O, Kergoat L, Hiernaux P, Guichard F, Mougin E, Timouk F, Lavenu F (2008) Analysis of the in situ and MODIS albedo variability at multiple timescales in the Sahel. J Geophys Res Atmos 113:D14

Simon MF, Pennington T (2012) Evidence for adaptation to fire regimes in the tropical savannas of the Brazilian Cerrado. Int J Plant Sci 173(6):711–723

Skamarock WC, Klemp JB, Dudhia J, Gill DO, Barker DM, Duda MG, Huang X-Y, Wang W, Powers JG (2008) Description of the advanced research WRF version 3. NCAR technical note. NCAR/TN–475 + STR. http://opensky.ucar.edu/islandora/object/technotes:500. Accessed June 2008

Tummon F, Solmon F, Liousse C, Tadross M (2010) Simulation of the direct and semidirect aerosol effects on the southern Africa regional climate during the biomass burning season. J Geophys Res 115. https://doi.org/10.1029/2009JD013738

United Nations, Department of Economic and Social Affairs, Population Division (2015) World population prospects: the 2015 revision, methodology of the United Nations Population Estimates and Projections. ESA/P/WP.242

Van de Vijver C, Foley CA, Olff H (1999) Changes in the woody component of an East African savanna during 25 years. J Trop Ecol 15:545–564

van der Werf GR, Randerson JT, Giglio L, Collatz GJ, Mu M, Kasibhatla PS, Morton DC, DeFries RS, Jin Y, van Leeuwen TT (2010) Global fire emissions and the contribution of deforestation, savanna, forest, agricultural, and peat fires (1997–2009). Atmos Chem Phys 10:11707–11735. https://doi.org/10.5194/acp-10-11707-2010

Wilson AM, Latimer AM, Silander JA Jr (2015) Climatic controls on ecosystem resilience: postfire regeneration in the Cape Floristic Region of South Africa. Proc Natl Acad Sci 112:9058–9063. https://doi.org/10.1073/pnas.1416710112

Wu L, Su H, Jiang JH (2011) Regional simulations of deep convection and biomass burning over South America: 2. Biomass burning aerosol effects on clouds and precipitation. J Geophys Res 116. https://doi.org/10.1029/2011JD016106

Xue Y, Sellers PJ, Kinter JL, Shukla J (1991) A simplified biosphere model for global climate studies. J Clim 4(3):345–364

Zhan XW, Xue YK, Collatz GJ (2003) An analytical approach for estimating CO_2 and heat fluxes over the Amazonian region. Ecol Model 162(1–2):97–117